A Magnetometer-Free Indoor Human Localization Based on Loosely Coupled IMU/UWB Fusion

Shaghayegh Zihajehzadeh, *Student Member*, *IEEE*, Paul K. Yoon, *Student Member, IEEE* and Edward J. Park, *Senior Member*, *IEEE*

***Abstract*— The magnetic distortions in indoor environment affects the accuracy of yaw angle estimation using magnetometer. Thus, the accuracy of indoor localization based on inertial-magnetic sensors will be affected as well. To address this issue, this paper proposes a magnetometer-free solution for indoor human localization and yaw angle estimation. The proposed algorithm fuses a wearable inertial sensor consisting of MEMS-based accelerometer and gyroscope with a portable ultra-wideband (UWB) localization system in a cascaded two-step filter consisting of a tilt Kalman filter and a localization Kalman filter. By benchmarking against an optical motion capture system, the experimental results show that the proposed algorithm can accurately track position and velocity as well as the yaw angle without using magnetometer.**

I. Introduction

Indoor localization and motion capture (MoCap) have numerous applications in medicine, rehabilitation [1] and sports science [2]. Due to the small size and light weight, a MEMS-based wearable inertial measurement unit (IMU) consisting of accelerometers, gyroscopes and magnetometers has been widely used for localization purposes [3]. However, although accurate for short period of time, the navigation solution based on MEMS-IMU will drift over time due to the IMU's inherent errors [3]. While the use of zero velocity update (ZUPT) will improve the localization accuracy for a shoe-mounted IMU, the drift will still appear over time and get worse for dynamic activities with less apparent ground contact [4]. Thus, to improve the indoor localization performance, absolute localization technologies based on vision and/or radio frequency (RF) [5] have been fused with IMU. However, vision based and RF based localization suffer from the non-line-of-sight (NLOS) problem and multipath effects respectively [5]. Among the RF based localization technologies, ultra-wideband (UWB) system can distinguish between the original and reflected signal by using narrow pulses (less than 1 ns) [5]. Due to the excellent precision, reasonable cost and low power consumption, UWB-based localization has become very popular [5]. A fused UWB/IMU localization system takes advantage of the high sampling rate of the IMU and the precision of the UWB system.

This work is supported by the Natural Sciences and Engineering Research Council of Canada (NSERC) and the experimental protocol (No, 2013s0750) is approved by the Office of Research Ethics of Simon Fraser University.

S. Zihajehzadeh, P. K. Yoon and E. J. Park are with the School of Mechatronic Systems Engineering, Simon Fraser University, 250-13450 102nd Avenue, Surrey, BC, Canada, V3T 0A3 (email: szihajeh@sfu.ca, pky@sfu.ca, ed_park@sfu.ca)

The available IMU/UWB fusion algorithms are divided into tightly coupled [6] and loosely coupled [7] based on whether the raw time of transmission data or the triangulated position data is used in IMU/UWB fusion. Similar to the GPS/IMU integration, a tightly coupled UWB/IMU fusion might be advantageous under UWB outages for outliers detection [6]. However, since UWB based localization has no line-of-sight requirements [5], UWB outages are less probable in a confined room environment. Furthermore, the loosely coupled approach offers simpler implementation and less computation. In the existing loosely coupled UWB/IMU fusion algorithms, magnetic data from magnetometer are used to help the estimation of yaw (heading) angle and thus the horizontal position and velocity [7],[8]. However, in indoor environments, the Earth's magnetic field can be easily perturbed by the presence of ferromagnetic objects [1][3][9], necessitating the need for magnetometer-free localization. Although a nonlinear tightly coupled Kalman filter-based fusion algorithm for magnetometer-free UWB/IMU integration has previously been proposed in [6], the complexity and computational costs of the nonlinear approach may not be desirable for low cost, battery powered ambulatory analysis in human localization [6].

This paper introduces a novel two-step cascaded Kalman filter for a loosely coupled magnetometer-free IMU/UWB integration. The study investigates the effect of not using magnetometer for indoor human localization and yaw angle estimation. The proposed algorithm uses two linear Kalman filters. At the first step, i.e. the tilt Kalman filter which is based on our algorithm in [10], tilt angles are estimated. At the second step, i.e. the localization Kalman filter, which is the main contribution of this paper, the UWB localization system is fused with the IMU's accelerometer and gyroscope to estimate position, velocity and the yaw angle. The experimental results show that the proposed method can accurately estimate yaw angle, and the position and velocity solutions match the ones from an optical MoCap system.

II. Method

In this work, a cascaded two-step Kalman filter is used to estimate the full 3-D orientation as well as the 3-D position and velocity. Euler angle representation is used to show the orientation of the sensor frame s (the coordinate system fixed to the IMU sensor) with respect to the navigation frame n (the coordinate system of UWB localization). The cascaded Kalman filter tends to be computationally more efficient than the centralized filters [2] and consists of a tilt angle Kalman filter and a localization Kalman filter. The structure of these filters is explained below.

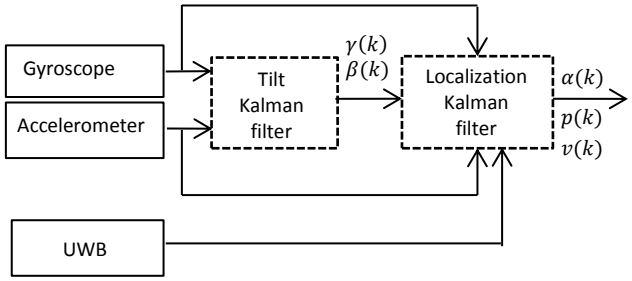

Fig. 1. Overview of the proposed algorithm structure

A. Tilt Kalman Filter

The tilt Kalman filter is based on our previous algorithm in [10], which allows accurate determination of roll and pitch angles. As shown in Fig. 1, in this filter, the tri-axial gyroscope and tri-axial accelerometer are used in a Kalman filter to estimate the normalized gravity vector in the sensor frame (i.e. the third row of the rotation matrix from the sensor frame to navigation frame ${}^{n}_{s}\boldsymbol{R}$):

$$ {}^{n}_{s}\boldsymbol{R} = \begin{bmatrix} c\alpha c\beta & c\alpha s\beta s\gamma - s\alpha c\gamma & c\alpha s\beta c\gamma + s\alpha s\gamma \\ s\alpha c\beta & s\alpha s\beta s\gamma + c\alpha c\gamma & s\alpha s\beta c\gamma - c\alpha s\gamma \\ -s\beta & c\beta s\gamma & c\beta c\gamma \end{bmatrix} \tag{1} $$

where α (yaw), β (pitch) and γ (roll) are the rotation angles about the Z-, Y-, and X- axes respectively.

Using the estimated last row of the rotation matrix, the desired roll and pitch angles can be calculated [10].

B. Localization Kalman Filter

The localization Kalman filter is designed to estimate position and velocity vectors as well as the first row of the rotation matrix ${}^{n}_{s}\boldsymbol{R}$. By estimating the first row of the rotation matrix and using the tilt angles information from the tilt Kalman filter, the yaw angle (α) can be estimated using:

$$ \alpha = \tan^{-1}\left(\frac{-c\gamma\ {}^{n}_{s}\boldsymbol{R}_{1,2} + s\gamma {}^{n}_{s}\boldsymbol{R}_{1,3}}{{}^{n}_{s}\boldsymbol{R}_{1,1}/c\beta}\right) \tag{2} $$

where ${}^{n}_{s}\boldsymbol{R}_{i,j}$ represents the i^{th} row and j^{th} column in rotation matrix ${}^{n}_{s}\boldsymbol{R}$.

As shown in Fig. 1, the localization Kalman filter uses the tri-axial gyroscope, tri-axial accelerometer and the UWB system in addition to the tilt angles information from the tilt Kalman filter. The following system model is used for the localization filter:

$$ \boldsymbol{x}(k+1) = \boldsymbol{A}(k)\,\boldsymbol{x}(k) + \boldsymbol{B}(k)\,\boldsymbol{u}(k) + \boldsymbol{n}(k) \tag{3} $$

$$ \boldsymbol{y}(k) = \boldsymbol{C}(k)\,\boldsymbol{x}(k) + \boldsymbol{w}(k) \tag{4} $$

where $\boldsymbol{x}$ is the state vectors; $\boldsymbol{A}$ is the state transition matrix; $\boldsymbol{B}$ is the input matrix; $\boldsymbol{u}$ is the input vector; $\boldsymbol{n}$ is the process noise vector; $\boldsymbol{y}$ is the measurement vector; $\boldsymbol{C}$ is the measurement matrix; and $\boldsymbol{w}$ is the measurement noise vector.

The state vector $\boldsymbol{x}(k) = [\boldsymbol{r}(k) \quad \boldsymbol{v}(k) \quad \boldsymbol{z}(k)]^T$ is the 9×1 vector where $\boldsymbol{r}$ and $\boldsymbol{v}$ are the 3-D position and velocity vectors, respectively; and $\boldsymbol{z}$ is the first row of the rotation matrix ${}^{n}_{s}\boldsymbol{R}$ and is equal to:

$$ \begin{gathered} \boldsymbol{z}(k) = [z_1 \quad z_2 \quad z_3] = \\ [c\alpha c\beta \quad c\alpha s\beta s\gamma - s\alpha c\gamma \quad c\alpha s\beta c\gamma + s\alpha s\gamma] \end{gathered} \tag{5} $$

The measurement vector $\boldsymbol{y}$, consists of the 3-D position and velocity measurements from the UWB system, i.e. $\boldsymbol{y}(k) = [\boldsymbol{r}_{UWB}(k) \quad \boldsymbol{v}_{UWB}(k)]^T$. Thus, $\boldsymbol{C}$ can be written as:

$$ \boldsymbol{C}(k) = [\boldsymbol{I}_{6\times6} \quad \boldsymbol{0}_{6\times3}] \tag{6} $$

Next, the following inertial navigation equations are used to calculate $\boldsymbol{A}$ and $\boldsymbol{B}$ matrices in the state space model (3):

$$ \boldsymbol{r}(k+1) = \boldsymbol{r}(k) + \Delta t\ \boldsymbol{v}(k) \tag{7} $$

$$ \begin{gathered} \boldsymbol{v}(k+1) = \\ \boldsymbol{v}(k) + \Delta t\ ({}^{n}_{s}\boldsymbol{R}(k)\boldsymbol{y}_A(k) - [0 \quad 0 \quad g]^T) \end{gathered} \tag{8} $$

$$ \boldsymbol{z}(k+1) = \boldsymbol{\Phi}(k)\,\boldsymbol{z}(k) \tag{9} $$

$$ \boldsymbol{\Phi}(k) = \boldsymbol{I}_{3\times3} - \Delta t\ \tilde{\boldsymbol{y}}_G(k) \tag{10} $$

where $\boldsymbol{y}_A(k) = [a_x \quad a_y \quad a_z]^T$ is the bias compensated output vector of the accelerometer; g is the norm of the gravity vector; $\tilde{\boldsymbol{y}}_G$ is the 3×3 skew symmetric matrix of tri-axial gyroscope measurements and $\boldsymbol{I}_{3\times3}$ is the 3×3 identity matrix. To find $\boldsymbol{A}$, $\boldsymbol{B}$ and $\boldsymbol{u}$, ${}^{n}_{s}\boldsymbol{R}(k)$ in Eq. (8) is re-written in terms of the three elements of the $\boldsymbol{z}$ vector and the known tilt angles from the tilt Kalman filter as following:

$$ {}^{n}_{s}\boldsymbol{R}(k) = \begin{bmatrix} z_1 & z_2 & z_3 \\ k_3(-k_1z_2 + k_2z_3) & k_2k_4(-k_1z_2 + k_2z_3) + k_4z_1/k_3 & k_1k_4(-k_1z_2 + k_2z_3) - k_2z_1/k_3 \\ -k_4 & k_2k_3 & k_1k_3 \end{bmatrix} \tag{11} $$

In Eq. (11), $k_1 = c\gamma$, $k_2 = s\gamma$, $k_3 = c\beta$ and $k_4 = s\beta$. By substituting Eq. (11) into Eq. (8) and expanding it, $\boldsymbol{A}$, $\boldsymbol{B}$ and $\boldsymbol{u}$ can be calculated as:

$$ \boldsymbol{A}(k) = \begin{bmatrix} \boldsymbol{I}_{3\times3} & \Delta t\,\boldsymbol{I}_{3\times3} & \boldsymbol{0}_{3\times3} \\ \boldsymbol{0}_{3\times3} & \boldsymbol{I}_{3\times3} & \boldsymbol{A}_{23}(k) \\ \boldsymbol{0}_{3\times3} & \boldsymbol{0}_{3\times3} & \boldsymbol{\Phi}(k) \end{bmatrix} \tag{12} $$

$$ \boldsymbol{A}_{23}(k) = \Delta t \begin{bmatrix} a_x & a_y & a_z \\ k_5 & k_6 & k_7 \\ 0 & 0 & 0 \end{bmatrix} \tag{13} $$

$$ \boldsymbol{u}(k) = [\boldsymbol{y}_A(k)^T \quad g]^T \tag{14} $$

$$ \boldsymbol{B}(k) = \begin{bmatrix} \boldsymbol{0}_{5\times4} \\ -\Delta t\ k_4 \quad \Delta t\ k_2k_3 \quad \Delta t\ k_1k_3 \quad -\Delta t \\ \boldsymbol{0}_{3\times4} \end{bmatrix} \tag{15} $$

where k_5 to k_7 are as following:

$$ \begin{aligned} k_5 &= a_y\,k_1/k_3 - a_z\,k_2/k_3 \\ k_6 &= -k_1k_3a_x - k_1k_2k_4a_y - k_1k_2k_4a_z \\ k_7 &= k_2k_3a_x + (k_2)^2k_4a_y + (k_2)^2k_4a_z \end{aligned} \tag{16} $$

The process and measurement noise covariance matrices in the tilt Kalman filter, $\boldsymbol{Q}(k)$ and $\boldsymbol{M}(k)$, are calculated using the following equations [2]:

$$\boldsymbol{Q}(k) = E[\boldsymbol{n}(k)\,\boldsymbol{n}(k)^T] = \tag{17}$$

$$\begin{bmatrix} \frac{1}{2}\Delta t^2\,\boldsymbol{I}_{3\times3} & \boldsymbol{0}_{3\times3} \\ \Delta t\,\boldsymbol{I}_{3\times3} & \boldsymbol{0}_{3\times3} \\ \boldsymbol{0}_{3\times3} & -\Delta t\,\tilde{\boldsymbol{z}}(k) \end{bmatrix} \begin{bmatrix} \boldsymbol{\Sigma}_A & \boldsymbol{0}_{3\times3} \\ \boldsymbol{0}_{3\times3} & \boldsymbol{\Sigma}_G \end{bmatrix} \begin{bmatrix} \frac{1}{2}\Delta t^2\,\boldsymbol{I}_{3\times3} & \boldsymbol{0}_{3\times3} \\ \Delta t\,\boldsymbol{I}_{3\times3} & \boldsymbol{0}_{3\times3} \\ \boldsymbol{0}_{3\times3} & -\Delta t\,\tilde{\boldsymbol{z}}(k) \end{bmatrix}^T$$

$$\boldsymbol{M}(k) = E[\boldsymbol{w}(k)\,\boldsymbol{w}(k)^T] = \begin{bmatrix} \sigma^2_{r,UWB}\,\boldsymbol{I}_{3\times3} & \boldsymbol{0}_{3\times3} \\ \boldsymbol{0}_{3\times3} & \sigma^2_{v,UWB}\,\boldsymbol{I}_{3\times3} \end{bmatrix} \tag{18}$$

where $\boldsymbol{\Sigma}_G$ and $\boldsymbol{\Sigma}_A$ are the covariance matrix of the gyroscope's and accelerometer's measurement noise respectively. By assuming that their noise variances for the gyroscope and accelerometer are equal to σ_G^2 and σ_A^2, $\boldsymbol{\Sigma}_G$ and $\boldsymbol{\Sigma}_A$ are set to $\sigma_G^2\boldsymbol{I}_{3\times3}$ and $\sigma_A^2\boldsymbol{I}_{3\times3}$; $\sigma^2_{r,UWB}$ and $\sigma^2_{v,UWB}$ are the UWB position and velocity noise variance respectively.

C. Smoothing

In this paper, the Rauch-Tung-Striebel (RTS) smoothing algorithm [2], a widely used smoothing algorithm in navigation applications, is utilized in the localization Kalman filter. RTS smoother recursively updates the smoothed estimate and its covariance in a backward sweep using the following equations:

$$\boldsymbol{K}_s(k) = \boldsymbol{P}^+(k)\,\boldsymbol{A}(k)\,[\boldsymbol{P}^-(k+1)]^{-1} \tag{19}$$

$$\boldsymbol{P}_s(k) = \boldsymbol{P}^+(k) + \boldsymbol{K}_s(k)\,[\boldsymbol{P}_s(k+1) - \boldsymbol{P}^-(k+1)]\,\boldsymbol{K}_s(k)^T \tag{20}$$

$$\boldsymbol{x}_s(k) = \boldsymbol{x}^+(k) + \boldsymbol{K}_s(k)\,[\boldsymbol{x}_s(k+1) - \boldsymbol{x}^-(k+1)] \tag{21}$$

where $\boldsymbol{P}^+$ and $\boldsymbol{P}^-$ are the "*a posteriori*" and the "*a priori*" covariance estimates; $\boldsymbol{K}_s$ is the smoother gain; $\boldsymbol{x}^+$ and $\boldsymbol{x}^-$ are the "a posteriori" and the "a priori" state estimates; and $\boldsymbol{x}_s$ is the smoothed state vector.

III. Experimental Setup

In order to evaluate the performance of the proposed algorithm, raw inertial data from Xsens MTx at the rate of 100 Hz are used. As shown in Fig. 2, the sensor is worn by a human subject on his waist. The MTx unit consists of tri-axial gyroscopes, tri-axial accelerometers and tri-axial magnetometers. The magnetometer data are only used for verification purposes. For the UWB-based localization system, the commercially available Ubisense Series 7000 is used. This system consists of four anchor nodes (sensors) and one mobile node (tag) which collects 3-D position data at the rate of about 10 Hz. The tag is attached to the subject's waist and the four UWB sensors are located at each corner of our $1.9 \times 2.3\ m$ rectangular-shaped test field. A Qualisys optical MoCap system, with the localization accuracy of 0.25 mm, is used as a reference motion tracking to provide ground truth position and velocity trajectories.

Since the inertial MoCap systems are comparatively less accurate under dynamic conditions [4], jumping activity is chosen to simulate highly dynamic motions in order to evaluate the performance of the proposed algorithm in the worst-case scenario. Thus, to collect experimental data, the subject is asked to jump from one corner of the rectangular test field to another and vice versa continuously for about 90 s. The experiment is repeated for nine times to carry out a statistical error analysis.

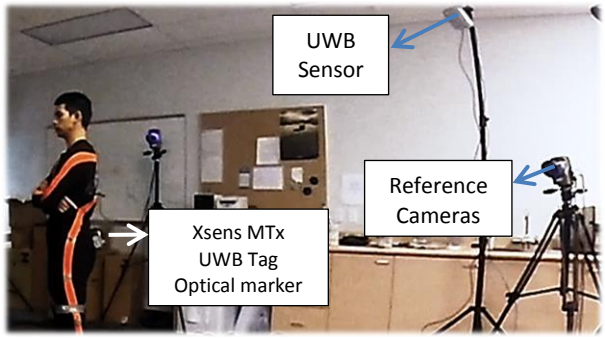

Fig. 2. Experimental setup: showing one corner of the test area

IV. Experimental Results and Discussion

In this section, performance of the proposed algorithm in yaw angle, position and velocity estimation is evaluated.

A. Yaw angle tracking

Fig. 3 shows the performance of our proposed algorithm for yaw angle estimation with and without RTS smoother. The reference yaw angle is calculated by employing magnetic data in addition to accelerometer and gyroscope measurements using our previously validated method in [10]. To ensure the accuracy of the reference curve, as shown in Fig. 3 (bottom), the experiment took place in a uniform magnetic field, away from electromagnetic disturbances. As it can be seen the blue curve in Fig. 3 (top), after about 20 s from the start of the motion the yaw angle which is initialized to zero will converge to the reference value. Additionally, by the use of smoother, the algorithm can correct for the initial estimation errors before convergence (the red curve in Fig. 3 (top)). Furthermore, the green curve in Fig. 3 (top) show the estimated yaw angle during a 20 s of simulated magnetic disturbance when raw magnetic data are fused with accelerometer and gyroscope. This magnetic disturbance is simulated based on the magnetic field data in proximity of an iron disk captured in our previous work [10]. This green curve verifies that the accuracy of the magnetometer aided estimation suffers in the presence of the magnetic disturbances, while the magnetometer-free solution does not get affected.

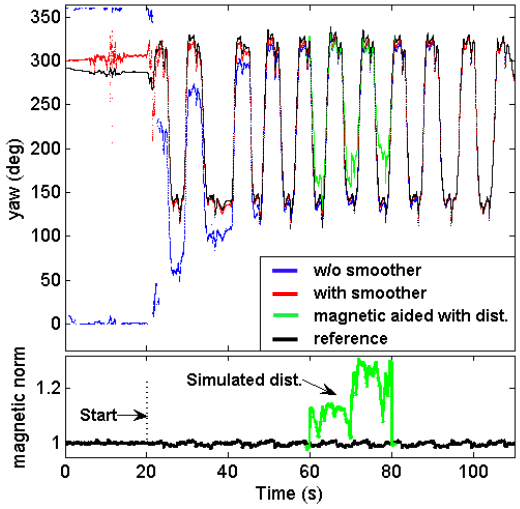

Fig. 3. Top: estimated yaw angle with and without smoother compared to the reference yaw angle, Bottom: normalized magnetic field norm

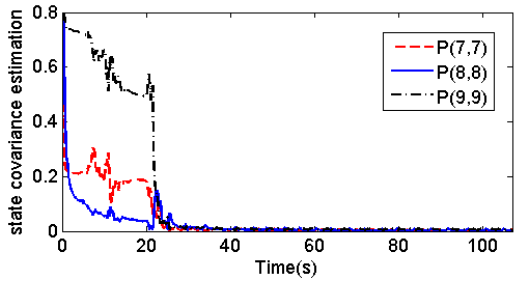

Fig. 4. State covariance estimation for the three elements of **z** vector

The time it takes for the estimated yaw angle to converge is due to the fact that the filter requires some motion to build the correlation between the states and correct for the initial unknown yaw angle. The same phenomena has been observed in [11] for GPS aided inertial navigation in outdoor environment. The state covariance estimation for the ***z*** vector in Fig. 4 also verifies that the covariance decreases rapidly after the start of the motion.

B. Position and velocity tracking

The estimated horizontal position for a part of experimental trial is shown in Fig. 5. As it can be seen in this figure, the fused solution can accurately track position and remove the inevitable drift in inertial tracking and the noise in UWB localization. The error analysis over the nine experimental trials shows that localization accuracy of the proposed method is less than $4\,cm$ in both x any y directions. Additionally, the horizontal velocity in Fig. 6

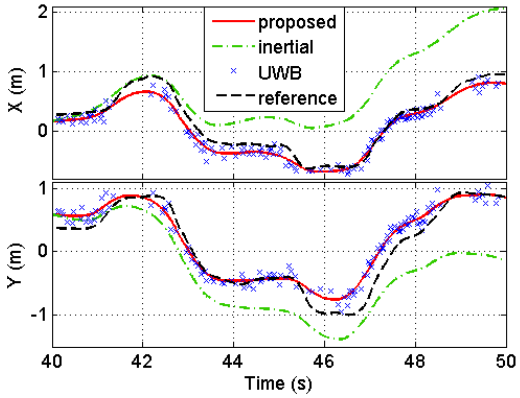

Fig. 5. Position trajectories in horizontal directions for a part of one experimental trial

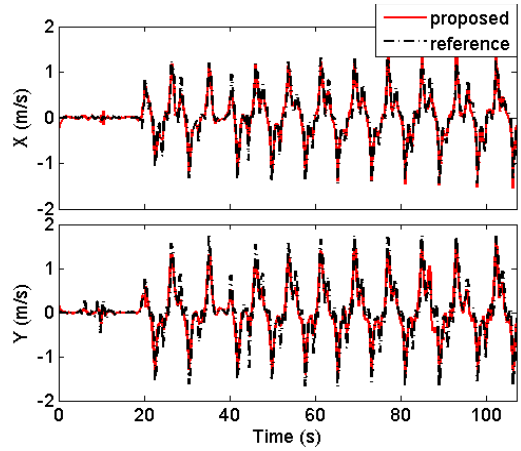

Fig. 6. Velocity trajectories in horizontal directions

shows that the algorithm can accurately track velocity during the experimental trials. Since the choice of not using magnetometer will not affect the position and velocity states in the vertical direction, the evaluation of these states was omitted from this study. Further analysis in the vertical direction has been done in our previous work [2].

V. Conclusion

This paper introduces a novel two-step cascaded Kalman filter for a loosely coupled magnetometer-free IMU/UWB integration for indoor human tracking. The algorithm consists of two linear Kalman filters: the tilt Kalman filter and the localization Kalman filter and is able to accurately estimate the tilt angles, position, velocity and the yaw (heading) angle. Compared to the magnetometer-aided tracking, using the proposed magnetometer-free algorithm, any indoor magnetic disturbances will no longer affect the horizontal position and velocity estimation. However, the experimental results show that about 20 s of motion is required for the yaw angle to converge which is the trade-off for not using the magnetometer. Benchmarking against the optical MoCap system, experimental results show that the horizontal position and velocity can be accurately tracked using the proposed method. In future, further experimentation will be performed to quantify the tracking improvement in the presence of real magnetic disturbances.

References

[1] S. House, S. Connell, I. Milligan, D. Austin, T. L. Hayes and P. Chiang, "Indoor Localization Using Pedestrian Dead Reckoning Updated with RFID-Based Fiducials," in *Conf. Proc. IEEE Eng. Med. Biol. Soc.*, Boston, MA, USA, Aug. 2011, pp. 7598–7601.

[2] S. Zihajehzadeh, T. J. Lee, J. K. Lee, R. Hoskinson, and E. J. Park, "Integration of MEMS Inertial and Pressure Sensors for Vertical Trajectory Determination," *IEEE Trans. Instrum. Meas.*, vol. 64, no. 3, pp. 804-814, Mar. 2015.

[3] S. Zihajehzadeh, D. Loh, T. J. Lee, R. Hoskinson, and E. J. Park, "A cascaded Kalman filter-based GPS/MEMS-IMU integration for sports applications," *Measurement*, vol. 73, pp. 200-210, Sept. 2015.

[4] X. Meng, Z. Q. Zhang, J. K. Wu, and W. C. Wong, "Hierarchical information fusion for global displacement estimation in microsensor motion capture.," *IEEE Trans. Biomed. Eng.*, vol. 60, no. 7, pp. 2052–63, Jul. 2013.

[5] Y. Gu, A. Lo, and I. Niemegeers, "A survey of indoor positioning systems for wireless personal networks," *IEEE Commun. Surv. Tutorials*, vol. 11, no. 1, pp. 13–32, Mar. 2009.

[6] J. D. Hol, F. Dijkstra, H. Luinge, and T. B. Schon, "Tightly Coupled UWB / IMU Pose Estimation." *Int. Conf. on Ultra-Wideband,* Vancouver, Canada, Sep. 2009, pp. 688 - 692.

[7] J. A. Corrales, F. A. Candelas, and F. Torres, "Sensor data integration for indoor human tracking," *Rob. Auton. Syst.*, vol. 58, no. 8, pp. 931–939, Aug. 2010.

[8] S. Pittet, V. Renaudin, B. Merminod, and M. Kasser, "UWB and MEMS Based Indoor Navigation," *J. Navig.*, vol. 61, no. 03, pp. 369-384, Jun. 2008.

[9] T. H. Riehle, S. M. Anderson, P. A. Lichter, N. A. Giudice, S. I. Sheikh, R. J. Knuesel, D. T. Kollmann, D. S. Hedin, and A. P. Hardware, "Indoor Magnetic Navigation for the Blind," in *Conf. Proc. IEEE Eng. Med. Biol. Soc.*, San Diego, CA, USA, Aug. 2012, pp. 1972–1975.

[10] S. Zihajehzadeh, D. Loh, M. Lee, R. Hoskinson, and E. J. Park, "A Cascaded Two - Step Kalman Filter for Estimation of Human Body Segment Orientation Using MEMS - IMU," in *Conf. Proc. IEEE Eng. Med. Biol. Soc.*, Chicago, Illinois, Aug. 2014, pp. 6270-6273.

[11] A. Waegli, J. Skaloud, P. Tomé, and J. Bonnaz, "Assessment of the Integration Strategy between GPS and Body-Worn MEMS Sensors with Application to Sports," in *Conf. Proc. ION GNSS*, Texas, USA, Sep. 2007.